




# Analysis of the bonding's energy in metal-halide perovskites and brief evaluation of meta-GGA functionals TPSS and revTPSS

José Juan Díaz<sup>1,\*</sup>, Iván Ornelas-Cruz<sup>1</sup>, Francisco J. Cano<sup>1,2</sup> , S. Velumani<sup>3</sup>, Salvador Gallardo-Hernández<sup>4</sup>, Iouri Koudriavtsev<sup>5</sup>, and Svetlana Mansurova<sup>6</sup>

<sup>1</sup> Programa de Nanociencias y Nanotecnología, CINVESTAV-IPN, Av. IPN 2508 Col. San Pedro Zacatenco, 07360 Ciudad de Mexico, Mexico

<sup>2</sup> Institute of Molecular and Materials of Le Mans e UMR-CNRS 6283, Le Mans Université, 70285 Le Mans, France

<sup>3</sup> J. Mike Walker '66 Department of Mechanical Engineering, Texas A&M University, College Station, TX 77843, USA

<sup>4</sup> Departamento de Física, CINVESTAV-IPN, Av. IPN 2508 Col. San Pedro Zacatenco, 07360 Ciudad de Mexico, Mexico

<sup>5</sup> Departamento de Ingeniería Eléctrica (SEES), CINVESTAV-IPN, Av. IPN 2508 Col. San Pedro Zacatenco, 07360 Ciudad de Mexico, Mexico

<sup>6</sup> Departamento de Óptica y Electrónica, Instituto Nacional de Astrofísica, Luis Enrique Erro 1, Tonantzintla, 72840 Heroica Puebla de Zaragoza, Puebla, México

**Received:** 3 October 2023

**Accepted:** 12 January 2024

**Published online:**

9 February 2024

© The Author(s), 2024

## ABSTRACT

Metal-halide perovskites, known for their remarkable photovoltaic performance and ease of production, have garnered global attention in material science. Addressing scalability requires tackling the technology's primary challenge: instability. Crucial insights into the complex chemistry of these materials are imperative for progress. The present study focused on well-known perovskites, namely CsPbI<sub>3</sub>, CH<sub>3</sub>NH<sub>3</sub>PbI<sub>3</sub> and HC(NH<sub>2</sub>)<sub>2</sub>PbI<sub>3</sub>. Through both cohesive energy and ICOHP analysis, the chemical bonding of these compounds. Additionally, a comparative evaluation of the functionals of TPSS, revTPSS, HCTH/407, and PBE was made through bandgap determination. The key findings of this study were: i) having confirmed the predominantly ionic nature of lead halide interactions; ii) having pointed out the predominantly covalent nature of the molecules' constituents binding; iii) having found that the strongest hydrogen bonds are formed by methylammonium; and iv) having nourished the utility of the TPSS meta-GGA functional in calculating the band gap of organic-inorganic perovskites. The results presented here could be important to the understanding and description of metal halide perovskite materials.

Handling Editor: Ghanshyam Pilania.

Address correspondence to E-mail: jose.diaz@cinvestav.mx

E-mail Addresses: franciscojavier.cano@outlook.es

<https://doi.org/10.1007/s10853-024-09381-2>

## Introduction

The search for a substitute or displacement of silicon technology in the photovoltaic field could be considered a revolution [1], which is more or less what perovskite solar cells (PSCs) are currently doing. The latter is reinforced by the fact that there is no other photovoltaic single-junction technology that could be comparable to established ones except for PSCs, even more, the latter has an advantage by the latter due to the band-gap tunability of metal-halide materials [2]. Unfortunately, lead-based perovskites are considered a danger to human health, because if this material degrades within a PSC, the amount of lead that would be released to the environment would be greater than the harmful threshold for human beings [3]. However, to the best of our knowledge, there is no other lead-free metal halide material that could compete with lead-based perovskites [4], as Fig. 1 shows.

Furthermore, the PCE growth ratio of PCS has decreased in the last five years: since their appearance in the “Notable exception” table from the periodic report of Green and co-workers in 2013, the average annual growth ratio was 10.4% [5–9] until 2018, but from 2018 to 2022 this ratio was 3.1% [10–14]. This mentioned decrement is natural considering that each year the PCE record of a PSC is closer to the Shockley-Queisser (SQ) limit: At present, the PCE record (25.7%) of a PSC [4] represents 86% of its SQ limit (which is 31.2% [15], considering a band gap

of 1.54 eV for  $\text{HC}(\text{NH}_2)_2\text{PbI}_3$ ). Therefore, within this context and taking into account that the first rung of the stability-improvement ladder of metal halide (MH) perovskites is the study of these materials at the nanoscale or atomic scale [1, 16, 17], the community has time to continue scrutinizing these materials using first-principles calculations, which in turn gives the possibility to further solidify even more the theoretical background, foster the discovery of new absorbers, and enhance those that already exists in this field.

First-principles calculations have been determinant on the understanding of the chemical and physical properties of MH perovskites (or simply MHP) with chemical formula  $\text{ABX}_3$ :  $\text{A} = \text{Cs}^+$ ,  $\text{CH}_3\text{NH}_3^+$  (MA), or  $\text{HC}(\text{NH}_2)_2^+$  (FA);  $\text{B} = \text{Sn}^{2+}$  or  $\text{Pb}^{2+}$ ; and  $\text{X} = \text{Cl}^-$ ,  $\text{Br}^-$ , or  $\text{I}^-$ . Among the great and vast studies that have been performed, special attention has been paid to the interaction between organic cations and the MH environment, where Van der Waals (vdW) interactions acquire a major role in these compounds, since they provide stability and can tune optoelectronic properties by bending the B–X bonds [20–26].

MH bonds have also been addressed, particularly by means of crystal orbital Hamiltonian Population (COHP) analysis, in such a way that the energy variation of the integrated COHP (ICOHP) could be tracked when alloys are studied [27]; in fact, a correlation between the ICOHP and bulk modulus (as expected) [28, 29]. However, MH bonds are well known for being more ionic in nature than covalent in nature

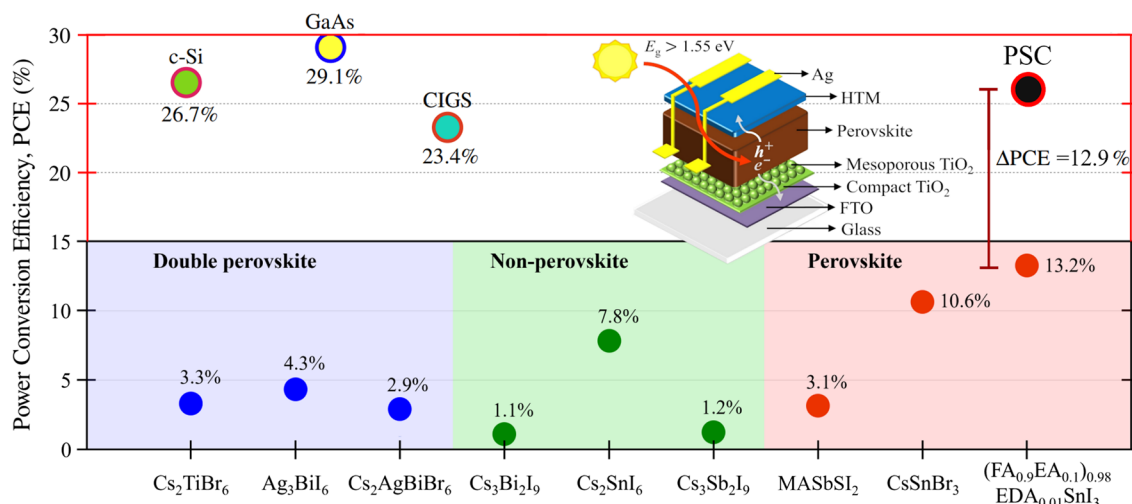


**Figure 1** Brief comparison of the power conversion efficiency (PCE) among some lead-free metal-halide absorbers with conventional technologies and the actual record of PSC devices

(achieved with a perovskite material with lead content). References [2, 18, 19] have been used for this purpose. Reference [4] has been used as inspiration for this figure.

[30], leaving the ionic part without being addressed. In either case, it is important to generate or have as many descriptors as possible to count with the necessary tools to seek the enhancement (or discovery) of materials for a particular applicability [1].

On the other hand, determining the band-gap energies has been a problem through the years on metal-halide perovskites. Experimentally, different band gaps have been determined in these materials, when they have played the role of absorber in solar cells [19]. Since the band gap of the absorber film determines the efficiency that the photovoltaic device could achieve, knowing this energy value is crucial.

In this work, a model to quantify the sum of the energy of the interaction of the *A*-site cation with the octahedral array and the binding of the chemical species constituting the cation is proposed. The use of charged periodic structures was avoided, and the energy attributed to the lead-halide bonds was first calculated to obtain the previously mentioned above.

Finally, to point out the utility of using meta-GGA functionals for the calculation of the band gap in metal-halide perovskites, a brief analysis of this matter was made through the TPSS, revTPSS, HCTH/407, and PBE functionals. On the basis of the presented results, in addition to the well-established functionals employed in the literature for the determination of the band gap of these materials, because of the level of theory they possessed, the TPSS one would be another option for this purpose.

## Methodology

### Computational details and model

All first-principles calculations were based on DFT as implemented in DMol<sup>3</sup> code [31]. To describe electron exchange and correlations, the functional proposed by Perdew, Burke, and Ernzerhof was employed [32], which is within the frame of the generalized gradient approximation (GGA). For the description of electrons, a basis set of doubled numerical orbitals with *d*-polarization functions, identified as DND within DMol3, was used [31, 33]. For geometrical optimization processes, all electrons from H, C, and N atoms were considered, and for semi-local pseudo potentials conserved by the norm of Cs, Pb, and I [34] were considered instead. Scalar relativistic (SR) corrections were taken into account for core electrons in all chemical

species [33], and all numerical orbitals reached zero after 6.9 Å. All the systems were fully relaxed until all internal forces were below  $7.0 \times 10^{-4}$  Ha/Å ( $\approx 1.9 \times 10^{-2}$  eV/Å); furthermore, to sample the first Brillouin zone in the reciprocal space, a  $4 \times 4 \times 3$  grid was used through the methodology of Monkhorst and Pack [35]. On the other hand, all numerical orbitals were equal to zero at 7.1 Å and a  $6 \times 6 \times 4$  k-mesh was employed for both energy and electronic properties calculations. To perform a comparison between meta-GGA and GGA functionals, in addition to the PBE functional, the TPSS [36], revTPSS [37], and HCTH/407 [38] ones were employed to calculate the band gap energies.

In order to correctly describe interactions within the crystal and due to both hydrogen and halogen bonds, corrections for dispersion interactions were considered by means of the Tkatchenko-Scheffler approach [39]. To complement the study, a crystal orbital Hamiltonian Population (COHP) [40] analysis was performed, in order to determine the integrated COHP (ICOHP) of the different interactions within the crystal solids to quantify the covalent contributions within the atomistic models studied [41, 42].

However, only tetragonal structures were taken into account throughout the calculations (Fig. 2). It is well known that MAPbI<sub>3</sub> (herein simply MAPI) has a tetragonal phase at room temperature ( $180 \text{ K} < T < 352 \text{ K}$ ) [43], nevertheless, both CsPbI<sub>3</sub> and FAPbI<sub>3</sub> (referred as CsPI and FAPI, respectively, from now on) do not crystallize in a tetragonal phase [44, 45]. The cubic phase of both CsPI and FAPI [44, 46] was employed to construct the tetragonal unit cell (UC), since the former could obtain this highly symmetric

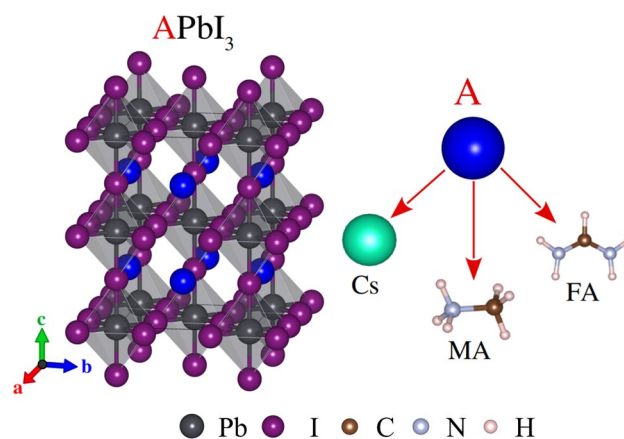


**Figure 2** The tetragonal unit cell is used for the APbI<sub>3</sub> perovskite; it is composed of four times the chemical formula.

phase at 634 K [45] and the latter above room temperature (390 K) [47]. Nevertheless, both cubic phases could be obtained by a careful synthesis process with special treatments to help the crystal endure through time and retain its perovskite structure [46, 48].

Figure 2 illustrates the unit cell (UC) of the perovskite systems used in this study. Regarding the description of the lattice constants ( $a_0$ ,  $b_0$ , and  $c_0$ ), the relative error (RE) was less than 2% for both MAPI and FAPI. In the case of CsPI, only the lattice constant  $a_0$  slightly deviated from the experimental value, with an RE of 5.1%. However, it had the smallest deviation from the experimental volume per unit cell (RE = 0.9%). In this regard, the equilibrium volume for the remaining compounds, MAPI and FAPI, yielded RE values of 4.4% and 1.2%, respectively.

Additionally, the averaged Pb–I bond lengths in CsPI, MAPI, and FAPI exhibited an RE of  $\leq 2.5\%$ . Therefore, the structural description of all perovskites is consistent with the methodology and the level of theory employed in this study [49]. Further structural details can be found in the supporting information document.

### Approach to quantifying the energy of the interactions within the perovskites

In the work of Svane et al. [21] it was adopted the convention that the interaction of the A-site cation is composed by the sum of the mono-pole term and the hydrogen bond (referred herein as HB). Besides, by definition the HB is decomposed in three interactions: the electrostatic and covalent ones, and the interaction originated from dispersions. Thus, since all calculations regarding dispersion interactions, which were added to the total electronic energy of each system, the energy attributed to them is immersed in any energy computation performed in this work. Furthermore, the monopole term from the approach of Svane and co-workers plays the role of the electrostatic part mentioned above, and by means of the ICOHP analysis, it is possible to find the energy attributed to the covalent part of the HB.

On the other hand, we can define an energy  $E(E_i^A + E_b^A)$ , i.e., the energy attributed to the sum of the

interaction energy of the A-site cation within the octahedra array,  $E_i^A$ , and in case it is a poli-atomic cation with an effective charge associated,  $E_b^A$  is the binding energy of the A-site cation. Therefore, decomposing  $E(E_i^A + E_b^A)$  in an ionic and a covalent part:

$$E(E_i^A + E_b^A) = E_i^A + E_b^A = E_{i-ion}^A + E_{b-ion}^A + E_{i-cov}^A + E_{b-cov}^A \quad (1)$$

As it could be seen from Eq. (1), it has been considered that both terms,  $E_i^A$  and  $E_b^A$ , have an ionic ( $E_{i-ion}^A$  and  $E_{b-ion}^A$ ) and a covalent part ( $E_{i-cov}^A$  and  $E_{b-cov}^A$ ). The latter is true since all chemical bondings could be structured just as the HB, but with major energy contributions proportional to the orbital interactions from the interacting chemical species and the inherent electrostatic forces (as a reminder, dispersion corrections were added to the total energy of all systems through all the calculations).

Thus, based on the work of Svane et al. [21], one can propose an equation that approximates the energy of the lead-iodide bonds of the  $APbI_3$  perovskite. First, we need to consider a system with  $Cs^+$  cations placed in the center of the cubo-octahedral cages of the relaxed  $APbI_3$  perovskite structures (Fig. 3). Now, if the energy of this system is calculated through a self-consistent process to relax only the orbitals, we can obtain the cohesive energy of the system, named  $E_{coh}^{Cs \cdot PbI_3}$ . Nevertheless, it is pertinent to subtract the energy related to the interaction between the spherical cations and the cubo-octahedral environment. By means of an ICOHP analysis, the energy attributed to the interaction between the orbitals of Cs and I atoms can be obtained, i.e., the covalent part of the interaction between Cs and I atoms. If the latter energy is labeled as  $E_{i-cov}^{Cs}$ , it is possible to define the binding energy of the MH bonds of the  $APbI_3$  perovskite, or simply  $E_b^{MH}$ , as:

$$E_b^{MH} = E_{coh}^{Cs \cdot PbI_3} - E_{i-cov}^{Cs} \quad (2)$$

To avoid any ambiguity, the binding energy of a poli-electronic system,  $E_b^{sys}$ , is calculated by means of:

$$E_{coh}^{sys} = E^{sys} - \sum_i n_i E_{atom}^i \quad (3)$$

where  $E^{sys}$ ,  $E_{atom}^i$ , and  $n_i$  are the total (electronic) energy of the system, the total (electronic) energy of the atom  $i$ , and the number of atoms  $i$  within the UC of the system at issue, respectively. Now, by means of Eqs. (2)



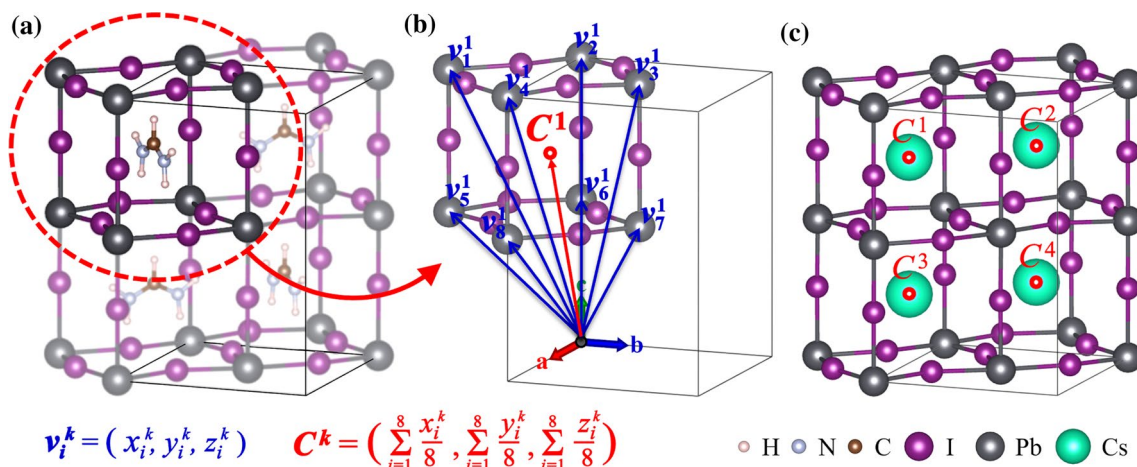


**Figure 3** **a** View of the four cages that the UC of APbI<sub>3</sub> (A=FA, for this particular case) has, one of these cages is highlighted with a red circle. **b** Vectors related with the positions of the lead atoms ( $\mathbf{v}_i^k$ ) that were used to calculate the vector asso-

ciated to the center of the cage ( $\mathbf{C}^k$ ). **c** Visualization of the four cages of the UC of A PbI<sub>3</sub> with the Cs atoms placed at their centers ( $\mathbf{C}^k$ ).

and (3), we can calculate the energy  $E(E_i^A + E_b^A)$ .  $E(E_i^A + E_b^A)$  is defined in Eqs. (4a) and (4b) as follows:

$$E(E_i^A + E_b^A) = \frac{1}{4} (E_{coh}^{APbI_3} - E_b^{MH}) \tag{4a}$$

$$E(E_i^A + E_b^A) = \frac{1}{4} [E_{coh}^{APbI_3} - (E_b^{Cs-PbI_3} - E_{i-cov}^{Cs-PbI_3})] \tag{4b}$$

In both equations Eqs. (4a) and (4b), the proportionality constant  $\frac{1}{4}$  was included since the chemical formula is present four times within all UCs, i.e., the energy values are given in energy units per formula unit (i.e., eV/f.u.). In addition, for the CsPI perovskite only,  $E(E_i^A + E_b^A)$  would be describing the interaction of the non-centered Cs<sup>+</sup> cations within the lead-halide environment, i.e., considering  $A = Cs$ , Eq. (3) would be describing only  $E(E_i^{Cs})$ , since  $E_b^{Cs} = 0$  in the CsPI perovskite.

## Results and analysis

### Energy of the interactions within the perovskites

Table 1 contains the energies related to the MH bonds of the perovskites CsPI, MAPI, and FAPI, in

**Table 1** Cohesive energy ( $E_{coh}^{APbI_3}$ ) and binding energies of the MH bonds ( $E_b^{MH}$ ) of all three perovskites CsPI, MAPI, and FAPI

Perovskite	$E_{coh}^{APbI_3}$	$E_b^{MH}$	$E_{b-cov}^{MH}$	$E_{coh}^{Cs-PbI_3}$	$E_{i-cov}^{Cs-PbI_3}$
CsPI	-58.63	-56.02	-16.21	-58.06	-2.04
MAPI	-156.19	-55.92	-15.37	-58.07	-2.15
FAPI	-166.47	-55.89	-15.27	-58.01	-2.13

For comparison, the covalent parts of the binding energies of the MH bonds ( $E_{b-cov}^{MH}$ ) are also shown, as well as the energy terms employed to obtain through Eq. (4b). All energy values are given in eV per UC (eV/UC)

**Table 2**  $E(E_i^A + E_b^A)$  energies obtained for CsPI, MAPI, and FAPI, with their corresponding covalent contributions due to both the interaction with the metal-halide array ( $E_{i-cov}^A$ ) and binding of the molecule's constituents ( $E_{b-cov}^A$ )

Perovskite	$E(E_i^A + E_b^A)$	$E_{i-cov}^A + E_{b-cov}^A$	$E_{i-cov}^A$	$E_{b-cov}^A$
CsPI	-0.65	-0.56	-0.56	0.00
MAPI	-25.07	-21.18	-1.75	-19.42
FAPI	-27.64	-26.85	-1.36	-25.50

All energy values are given in eV per f.u (eV/f.u.)

conjunction with their respective cohesive energies. Table 2 shows the energies related to the A-site cations, and in Fig. 4 some of the energies are plotted and a special attention was paid to the HBs within the organic-inorganic systems.

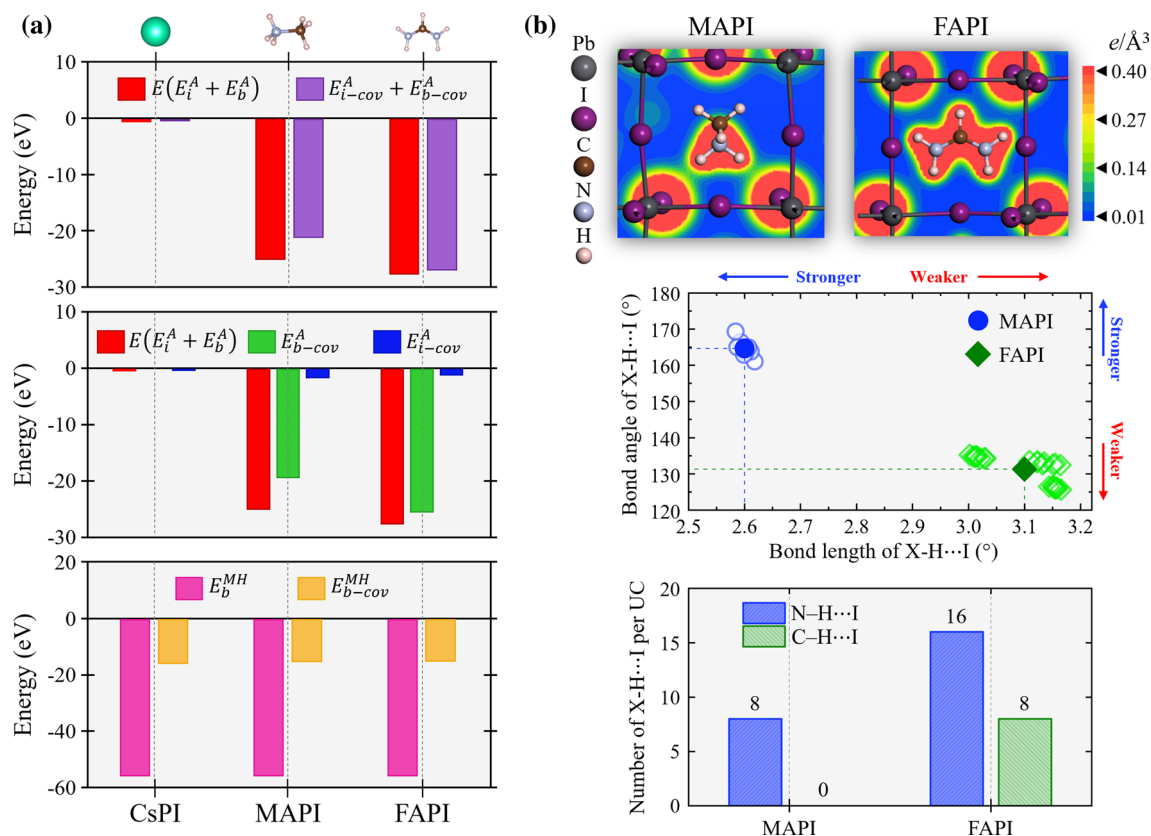


**Figure 4** **a** Comparison between the calculated energies shown in Tables 1 and 2 and calculated using Eqs. (2), (3), (4). **b** From top to bottom: i) electronic charge density comparison between MAPI and FAPI reflecting the concentration of charge between the organic cations and halogens; ii) bond angles and bond

lengths of the X-H...I HBs in both MAPI and FAPI, average values are shown with filled symbols; iii) number of X-H...I HBs per UC in both MAPI and FAPI; all bond lengths that fulfilled the X-H...I < 3.2 Å criteria [54], were considered as HB bond.

By analyzing the data in Table 1, it could be seen that the cohesive energies reflected the covalent bonds present in the molecules within the organic-inorganic compounds, due to the lower energy values obtained for these systems in comparison to the all-inorganic one. Further, the lowest energy value was obtained in FAPI, due to the stronger covalent bonds in the FA<sup>+</sup> cations, because of the N–C–N bond, in comparison to the MA<sup>+</sup> ones, which only possess a C–N bond. All the above-mentioned are in good agreement with previous theoretical calculations. For example, Santos et al. [50] obtained a cohesive energy of 157.92 eV for MAPI, only 1.73 eV (or 36 meV/atom) above the result presented in Table 1. Furthermore, in that same work, a cohesive energy of 55.54 eV was computed for CsPI, 3.09 eV (155 meV/atom) above the result presented in Table 1 for the all-inorganic perovskite. In addition, that same work supports a stronger cohesive energy

in perovskites with FA content than in those with MA cations within the perovskite structure.

The energy discrepancies addressed above could be related to the three main things: i) distinct approaches to describe the valence electrons (PAW method *vs.* pseudopotentials), ii) distinct corrections for dispersion interactions (TS *vs.* D3), and iii) distinct atomistic models to describe the perovskite compounds (super-cubic structures were used by Santos and co-workers, constituted by eight formula units, which means additional interactions between the chemical constituents within the UC).

On the other hand, previous studies have pointed out that in organic-inorganic perovskites the major contribution to the cohesive energy of the material comes from the organic part, rather than the inorganic one [50]. As we can see from the  $E_b^{MH}$  values of both MAPI and FAPI, the binding energy associated to the metal-halide bonds only represents around 35% of

the total energy related to the bonds of the crystal, in agreement with the literature. However, in CsPI, the difference between  $E_{coh}^{APbI_3}$  and  $E_b^{MH}$  is only 2.61 eV, which is related to the energy of the interaction between the off-centered  $Cs^+$  cations and the metal-halide environment. Furthermore, in the all-inorganic perovskite where the stronger lead-iodide bonds are found, which could be supported by the fact that this perovskite possessed the most distorted octahedral array among the three perovskites studied (see supporting information), in agreement with the literature [51]. In fact, our optimized structures met the expected increasingly octahedral distortion as the volume of the *A*-site cation decreases [23].

Thus, in CsPI the stabilization of the orbitals from I and Pb could be ruled by Jahn–Teller effects, producing an increased interaction between the *I-p* and *Pb-s* orbitals. The binding energy of the metal halide array involves bonding *Pb-p-I-p* and antibonding *Pb-s-I-p* interactions in the bottom and top of the valence band, respectively [52] (see also Supporting Information document). In addition, the bond lengths are shorter in CsPI with respect to MAPI and FAPI, in fact, it was obtained an ascendant tendency on the average *Pb-I* bond length as the volume of the cation in the *A*-site increases (as expected). Thus, since there is also an increasingly tendency on the  $E_{b-cov}^{MH}$  values from CsPI to FAPI. Therefore, the covalent character in the metal halide arrays is regulated by the bonding *Pb-p-I-p* and antibonding *Pb-s-I-p* interactions' proportion, where short *Pb-I* bond lengths ( $\sim 3.16$  Å) favors the covalency but this is hindered by larger *Pb-I* bond lengths ( $\sim 3.24$  Å).

Finally, it could be seen that the energy values of  $E_{b-cov}^{MH}$  obtained for all systems, contribute around 28% to the binding energy of the metal-halide arrays, i.e., the binding nature of these chemical species is mostly ionic, in agreement with the literature since it has been widely recognized that the interaction between the metal and halogen atoms is mostly ionic [30].

Table 2 are presented the energy results for  $(E_i^A + E_b^A)$ , i.e., the energy attributed to the sum of the binding energy of the *A*-site cation and the interaction with its lead-iodide environment. First, as mentioned above, the energy obtained by the all-inorganic perovskite in this respect is associated exclusively with the interaction of the spherical monovalent cation with its environment. The result obtained here is of the same order as the energies previously quantified by

Ornelas-Cruz et al. [53] of the interaction between Cs and halogen atoms (0.06–0.18 eV), within all-inorganic tin-based mixed-halide perovskites. In that same work, the presence of charge between Cs and halide atoms pointed out a covalent interaction between them; in the present case, it is confirmed through Table 2 that 86% of such an interaction is indeed covalent.

In both organic-inorganic perovskites,  $E(E_i^A + E_b^A)$  energies are found to be two orders of magnitude higher than that of CsPI. In both MAPI and FAPI the majority of the energy associated with  $E(E_i^A + E_b^A)$ , 84 and 97%, respectively, were attributed to covalent interactions: between the molecule's constituents and between the molecule and its surrounding environment. Moreover, it has been confirmed that the species constituting FA molecules are more tightly bound than those in MA molecules. Interestingly, 50–61% of the total cohesive energy of the UC in the organic-inorganic perovskites is attributed to the energy of covalent bonds formed within the molecules, and only 3–4% belongs to the covalent interaction between the organic molecules and the cubo-octahedral periodic arrangement. Additionally, it is worthy to mention that by means of the ICOHP analysis and for the FAPI compound as well, it is reported in the literature an energy value of 1.26 eV/f.u., for the FA–I interaction, 0.1 eV/f.u. below the reported value in Table 2, which reinforces the reliability of the methodology here employed [27].

The main feature of the present methodology, in addition to avoiding the use of charged periodic systems on the computation of these energy values, is that having as reference both  $E_b^{MH}$  and  $E(E_i^A + E_b^A)$  it is possible to qualitatively address the energy contributions within the perovskite compounds. The ICOHP analysis has its roots in tight-binding theory [40], thus it is theoretically supported by quantum mechanics. Therefore, it is crucial to be coherent with the chemically expected description of a material when its study involves systems that has no physical meaning, such as those used for the calculation of  $E_{coh}^{Cs-PbI_3}$  and  $E_{i-cov}^{Cs-PbI_3}$ . Fortunately, in all three systems both terms,  $E_b^{MH}$  and  $E(E_i^A + E_b^A)$ , not only had lower energies than those obtained through ICOHP method, but also helped in pointing out where the ionic and the covalent interactions are crucial within the components of these

complex materials (see Fig. 4a to visualize this energy comparison).

One of the routes to improve the stability of the metal-halide perovskite materials is through chemical doping or chemical substitution. Complex perovskites are beyond the scope of this work; nevertheless, this qualitatively energetic approach can provide insights into the nature of chemical bonds. When a gradual chemical substitution of a specific chemical species is performed, it would be possible to track the modulation of the chemical bond character. However, conclusions about stability cannot be drawn solely from this study. Mechanical and vibrational first-principles analyses, as well as calculations of formation energies, are well-established theoretical methods for gaining insights into a material's stability [55–57]. Therefore, the present method serves as an additional tool for the comprehensive characterization of the absorber material of a PSC.

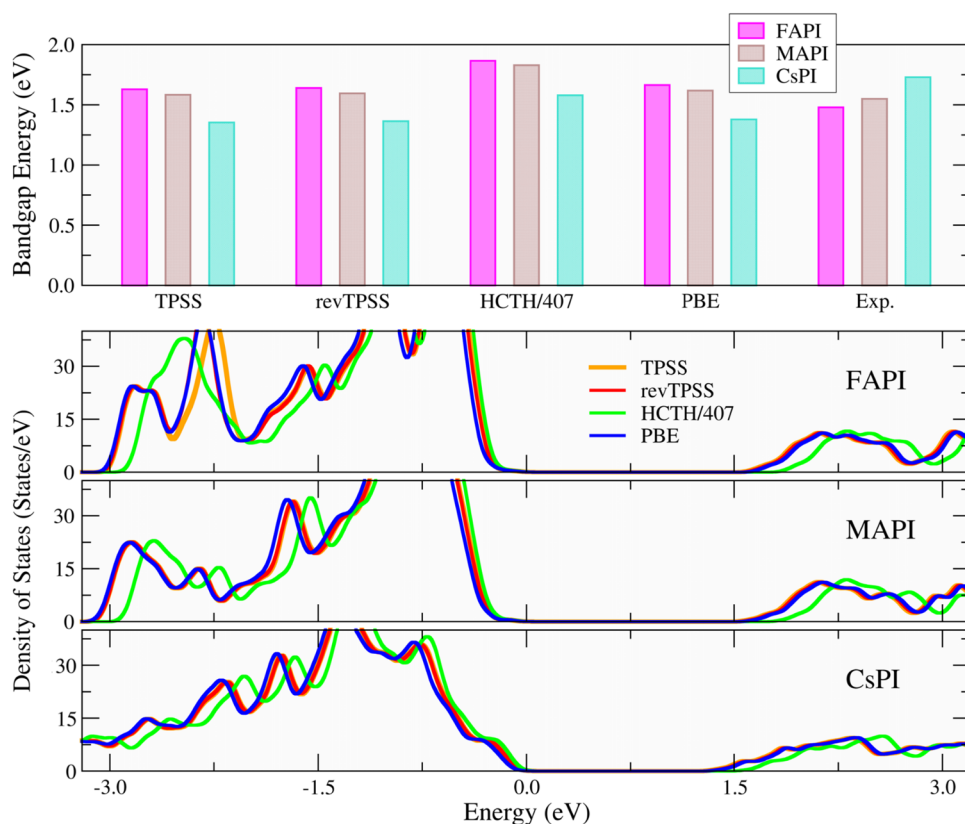
To complement the results presented in Table 2, special attention was paid to the HB in Fig. 4b. By counting only, the number of *reactive* HBs (i.e., N–H  $\cdots$  I) in both molecules, MA and FA, MAPI possess a smaller number of HBs per UC than FAPI (3 *vs* 4 per

formula unit), but due to the size and symmetry of FA molecule it is important to consider also C–H  $\cdots$  I interactions. Figure 4b shows the electronic charge density of both MAPI and FAPI in order to better visualize the HBs present in both structures. As observed, there is a higher concentration of charge in the N–H  $\cdots$  I HBs from MAPI compared to those from FAPI. Moreover, driven by the definition of the HB [58], there are two other properties that could give better insights on the HB strength: the X–H  $\cdots$  I bond angle and bond length. Shorter NH  $\cdots$  I means stronger HB and this strength is reinforced as N–H  $\cdots$  I approaches 180°. Thus, despite having more HBs in FAPI, the strongest ones are formed within MAPI, in good agreement with the energy value reported in Table 2.

### Electronic properties

As we can see from Fig. 5, the experimentally determined band gap of the metal-halide perovskites follows a descendant trend as the cation's volume in the *A*-site becomes greater: CsPI > MAPI > FAPI. Unfortunately, no similar trend was found for any

**Figure 5** Top: Comparison of the bandgap energies obtained with the different functionals employed in this work; all numeric values are given in the Supporting Information. Bottom: The density of states of the three different perovskite compounds studied in this work was obtained through the functionals TPSS, revTPSS, HCTH/407, and PBE.





of the functionals tested in this work, in fact the opposite trend in all cases. Nevertheless, it would be worth noting that the obtained band gap is of the direct type for all 4 functionals, consistent with the literature [59]. Similar results have been found in the literature [50], due to the sensibility of the band gap to the octahedral tilt and octahedral distortions [23]. The latter issue arises because the valence and conduction bands predominantly consist of electronic states from both Pb and I, and as we can see from the energetic values of Table 2, there is a different interaction between the Pb-*s* and Pb-*p* orbitals and the I-*p* ones in each perovskite system. From the computational calculations here performed, a stronger covalent interaction in the Pb-I bonds has produced a smaller bandgap, contrary to the trend found in conventional semiconductors (e.g. C, Si, Ge). Nevertheless, this might be related to the hybridization of I-*p* orbitals with those from the A-site cation, since there is an interaction between them, as Table 2 showed.

On the other hand, the greatest relative error found among the calculated bandgaps was on the HCTH/407 for the FAPI compound, in fact, from the results presented in Fig. 5, this GGA functional did not have a good precision in describing the bandgap of organic-inorganic perovskites. However, it was the best among all functionals for the all-inorganic perovskite, the bandgap determined with HCTH/407 was 0.15 eV below the experimental value. This result, is in good agreement with the literature, since the HCTH/407 functional has proven its feasibility in all-inorganic perovskites [29]. Additionally, the best results found for organic-inorganic perovskites were given by the TPSS functional: 0.03 and 0.15 eV above the experimental values of MAPI and FAPI, respectively. In this respect, previous first-principles studies have pointed out that both TPSS and revTPSS functionals were among the best existing within DFT, due to the precision of the description of the electronic density [60]. Thus, we do not discard the possibility that further improvements on the calculation of the band gap could be achieved with TPSS, e.g., by means of a greater basis set (considering empty *p* orbitals for H atoms) or all-electron calculations.

The approaches to address exchange and correlation interactions between both meta-GGA and hybrid functionals are different, while the former is a functional on the term kinetic energy density to further improve the descriptions of the variations on the electronic density, the latter describe part of the

exchange interactions through the exact functional given by the Hartree–Fock method [61]. Thus, different band gap energies are expected. As a consequence, hybrid functionals tend to widen the band gap due to the exchange description being done mainly on the Pb orbitals. For instance, Wang et al. [62] have reported for CsPI band gaps calculated by means of HSE06 and PBE0 equal to 2.19 and 2.83 eV while Santos et al. [50] have reported through the HSE06 functional band gaps of 2.20 and 2.08 eV for CsPI and MAPI, respectively. For comparison, the band gaps obtained here for CsPI and MAPI employing the TPSS functional are 1.35 and 1.58 eV, respectively.

On the other hand, based on the DOS graphs presented in Fig. 5, it is evident that the characterization of the electronic states in both the valence and conduction bands (VB and CB, respectively) varied slightly between different functionals. Nevertheless, the electronic states described by means of the PBE functional are very similar to those described by the revTPSS and TPSS ones, in both the VB and CB. For both MAPI and CsPI, it could be said that PBE provided a description of the electronic density of states at the level of meta-GGA functionals [63]. However, there is a peak in FAPI at approximately 2.5 eV that was shifted to higher energies through the TPSS functional. Thus, describing the electronic states resulting from the hybridization of N-*p*, I-*p*, and Pb-*p* orbitals can be challenging, even at the meta-GGA level, owing to the localization of N-*p* orbitals. Moreover, HCTH/407 described the distribution of the states through the energies of the bottom half of the VB, because of the states belonging to N-*p* orbitals from FAPI; besides, for the remaining perovskites (MAPI and CsPI), HCTH/407 displaced the localization of the states composing the VB.

While the discrepancies in the description of electronic states among different functionals are more evident in the DOS plots, the band gap ( $E_g$ ) is ultimately determined by the difference between the energy at the valence band maximum ( $E_{VBM}$ ) and that at the conduction band minimum ( $E_{CBM}$ ), expressed as  $E_g = E_{CBM} - E_{VBM}$ . To give an idea of these energy values, the relative band gaps ( $\Delta E_g$ ) in comparison to those obtained through the PBE functional ( $E_g^{PBE}$ ) were calculated by means of:  $\Delta E_g = E_g^i - E_g^{PBE}$ . Consequently, for TPSS, revTPSS, and HCTH/407, we obtained the following  $\Delta E_g$  values: - 0.03

to  $-0.04$  eV,  $-0.01$  to  $-0.03$  eV, and  $-0.20$  to  $-0.21$  eV, respectively.

Therefore, undoubtedly more testes should be done to determine which functional stands out among the others, however, some remarks can be extracted from this brief analysis: i) TPSS would be a good option for the description of the electronic properties of organic-inorganic metal-halide perovskites, ii) revTPSS and PBE functionals might deliver similar electronic descriptions on these types of compounds, and iii) HCTH/407 could give a good bandgap approximation in all-inorganic perovskites.

Finally, in Fig. 6, it is possible to observe that the *A*-site cation did not contribute to the top of the VB as expected [59]. Nevertheless, there are states from the *A*-site species in the energy region where the antibonding Pb-*s* and I-*p* interactions occur, thus, the presence of these states confirmed that lead-iodide orbitals are further hybridized with those from the *A*-site cations. In fact, the X–H  $\cdots$  I interactions generated bonding contributions in the VB in both MAPI and FAPI, while in CsPI the Cs-I interactions brought about bonding and antibonding ones in the same energy region (see Supporting Information). Thus, the HBs can counteract the weakening of the lead-iodine bonds originating from the antibonding interactions between the orbitals of their constituents. Lastly, because of the sharp peaks of the N-*p* orbitals, we might have these states well concentrated in FA molecules within the perovskite.

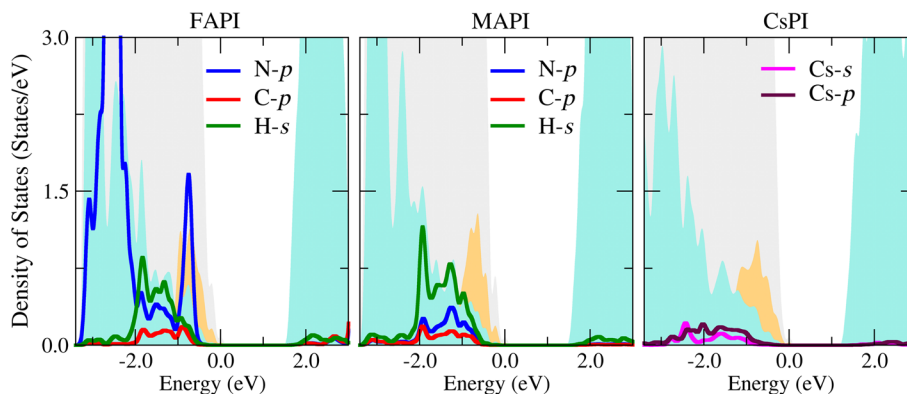
## Conclusions

We have performed a Density Functional Theory study on three well known perovskites, namely CsPbI<sub>3</sub>, CH<sub>3</sub>NH<sub>3</sub>PbI<sub>3</sub>, and HC(NH<sub>2</sub>)<sub>2</sub>PbI<sub>3</sub>. A qualitative analysis of the chemical bonding of their constituents was carried out by means of both the cohesive energy and COHP analysis to elucidate the covalent proportion of the interactions involved within the perovskite systems. We confirmed that most of the chemical bonding between the lead and halide species was attributed to ionic interactions. Furthermore, it was found that formamidinium molecules are more tightly bound than methylammonium ones, and the observed trend in the strength of the interaction between the cations and the cubo-octahedral cages was as follows. CH<sub>3</sub>NH<sub>3</sub><sup>+</sup> > HC(NH<sub>2</sub>)<sub>2</sub><sup>+</sup> > Cs<sup>+</sup>.

Based on bandgap calculations and density of states (DOS) analysis, it is concluded that the meta-GGA TPSS functional would be a good option for the band-gap description of organic-inorganic perovskites, while the GGA HCTH/407 functional would be a good choice for the band gap calculation in all-inorganic ones. Moreover, PBE and revTPSS functionals could deliver similar results in both DOS and band gaps, based on the systems here studied. The results obtained with respect to structural properties, cohesive energies, ICOHP energy values and bandgap energies, have been compared with previous theoretical and experimental results for two main reasons: the reproducibility of first-principles calculations and to deliver the correct description of the material. Therefore, due to the proximity found with previous results, the present work might be helpful for future studies.

In this respect, special attention should be paid to the energetical values of the cohesive energies, since,

**Figure 6** Density of states (DOS) of the orbitals from the chemical species constituting the *A*-site cations in all three perovskites studied and obtained by means of the PBE functional. DOS from the Pb-*s*, Pb-*p* and I-*p* orbitals are given in orange, turquoise, and light gray, respectively.



from a computational materials science perspective, it is an extensive property. In addition, the energy values calculated through the ICOHP analysis depend on the basis set employed. Despite having been cautious on meeting the chemically expected results, the methodology proposed here should be further tasted, especially in much more complex compounds such as those used in current PSC.

## Acknowledgements

José Juan Díaz (CVU: 716457) and F. J. Cano (CVU: 777801) acknowledge the Consejo Nacional de Humanidades, Ciencias y Tecnologías (CONAHCYT) for the doctoral grants awarded. I. O.-C. sincerely acknowledges J. J. D. and his advisors, I. K. and S. M., for the opportunity to collaborate on this work. I. O.-C. also acknowledges CINVESTAV-IPN, as all computational resources for this project were provided by this prestigious institution

## Author contributions

JJD: Conceptualization, Methodology, Investigation, Formal analysis, Software–Data Curation, Writing–Original Draft. IO: Conceptualization, Software–Data Curation. FJC: Investigation, Writing–Original Draft, Writing–Review & Editing. SG: Supervision, Visualization. YK: Supervision, Project administration. SM: Supervision, Project administration.

## Data availability

All data are available from the corresponding authors, please contact jose.diaz@cinvestav.mx

## Declarations

**Conflict of interest** The authors declare that they have no known competing financial interests or personal relationships that could have appeared to influence the work reported in this paper.

**Ethical approval** Not applicable. There are no experiments involving human tissue or any ethical issues.

**Supplementary Information** The online version contains supplementary material available at <https://doi.org/10.1007/s10853-024-09381-2>.

**Open Access** This article is licensed under a Creative Commons Attribution 4.0 International License, which permits use, sharing, adaptation, distribution and reproduction in any medium or format, as long as you give appropriate credit to the original author(s) and the source, provide a link to the Creative Commons licence, and indicate if changes were made. The images or other third party material in this article are included in the article's Creative Commons licence, unless indicated otherwise in a credit line to the material. If material is not included in the article's Creative Commons licence and your intended use is not permitted by statutory regulation or exceeds the permitted use, you will need to obtain permission directly from the copyright holder. To view a copy of this licence, visit <http://creativecommons.org/licenses/by/4.0/>.

## References

- [1] Curtarolo S, Hart GLW, Nardelli MB, Mingo N, Sanvito S, Levy O (2013) The high-throughput highway to computational materials design. *Nat Mater* 12:191–201. <https://doi.org/10.1038/nmat3568>
- [2] Almora O, Baran D, Bazan GC, Berger C, Cabrera CI, Catchpole KR, Erten-Ela S, Guo F, Hauch J, Ho-Baillie AWY, Jacobsson TJ, Janssen RAJ, Kirchartz T, Kopidakis N, Li Y, Loi MA, Lunt RR, Mathew X, McGehee MD, Min J, Mitzi DB, Nazeeruddin MK, Nelson J, Nogueira AF, Paetzold UW, Park N-G, Rand BP, Rau U, Snaith HJ, Unger E, Vaillant-Roca L, Yip H-L, Brabec CJ (2021) Device performance of emerging photovoltaic materials (version 2). *Adv Energy Mater* 11:2102526. <https://doi.org/10.1002/aenm.202102526>
- [3] Babayigit A, Ethirajan A, Muller M, Conings B (2016) Toxicity of organometal halide perovskite solar cells. *Nat Mater* 15:247–251. <https://doi.org/10.1038/nmat4572>
- [4] Ke W, Kanatzidis MG (2019) Prospects for low-toxicity lead-free perovskite solar cells. *Nat Commun* 10:965. <https://doi.org/10.1038/s41467-019-08918-3>

- [5] Green MA, Emery K, Hishikawa Y, Warta W, Dunlop ED (2013) Solar cell efficiency tables (version 42). *Prog Photovolt Res Appl* 21:827–837. <https://doi.org/10.1002/pip.2404>
- [6] Green MA, Emery K, Hishikawa Y, Warta W, Dunlop ED (2014) Solar cell efficiency tables (version 44). *Prog Photovolt Res Appl* 22:701–710. <https://doi.org/10.1002/pip.2525>
- [7] Green MA, Emery K, Hishikawa Y, Warta W, Dunlop ED (2015) Solar cell efficiency tables (version 46). *Prog Photovolt Res Appl* 23:805–812. <https://doi.org/10.1002/pip.2637>
- [8] Green MA, Emery K, Hishikawa Y, Warta W, Dunlop ED (2016) Solar cell efficiency tables (version 48). *Prog Photovolt Res Appl* 24:905–913. <https://doi.org/10.1002/pip.2788>
- [9] Green MA, Hishikawa Y, Warta W, Dunlop ED, Levi DH, Hohl-Ebinger J, Ho-Baillie AWY (2017) Solar cell efficiency tables (version 50). *Prog Photovolt Res Appl* 25:668–676. <https://doi.org/10.1002/pip.2909>
- [10] Green MA, Hishikawa Y, Dunlop ED, Levi DH, Hohl-Ebinger J, Ho-Baillie AWY (2018) Solar cell efficiency tables (version 52). *Prog Photovolt Res Appl* 26:427–436. <https://doi.org/10.1002/pip.3040>
- [11] Green MA, Dunlop ED, Levi DH, Hohl-Ebinger J, Yoshita M, Ho-Baillie AWY (2019) Solar cell efficiency tables (version 54). *Prog Photovolt Res Appl* 27:565–575. <https://doi.org/10.1002/pip.3171>
- [12] Green MA, Dunlop ED, Hohl-Ebinger J, Yoshita M, Kopidakis N, Hao X (2020) Solar cell efficiency tables (version 56). *Prog Photovolt Res Appl* 28:629–638. <https://doi.org/10.1002/pip.3303>
- [13] Green MA, Dunlop ED, Hohl-Ebinger J, Yoshita M, Kopidakis N, Hao X (2021) 6 Solar cell efficiency tables (Version 58). *Prog Photovolt Res Appl* 29:657–667. <https://doi.org/10.1002/pip.3444>
- [14] Green MA, Dunlop ED, Hohl-Ebinger J, Yoshita M, Kopidakis N, Bothe K, Hinken D, Rauer M, Hao X (2022) Solar cell efficiency tables (Version 60). *Prog Photovolt Res Appl* 30:687–701. <https://doi.org/10.1002/pip.3595>
- [15] Rühle S (2016) Tabulated values of the Shockley-Queisser limit for single junction solar cells. *Sol Energy* 130:139–147. <https://doi.org/10.1016/j.solener.2016.02.015>
- [16] Wimmer E (1996) Computational materials design and processing: perspectives for atomistic approaches. *Mater Sci Eng B* 37:72–82. [https://doi.org/10.1016/0921-5107\(95\)01459-4](https://doi.org/10.1016/0921-5107(95)01459-4)
- [17] Christians JA, Habisreutinger SN, Berry JJ, Luther JM (2018) Stability in perovskite photovoltaics: a paradigm for newfangled technologies. *ACS Energy Lett* 3:2136–2143. <https://doi.org/10.1021/acsenergylett.8b00914>
- [18] Green MA, Dunlop ED, Yoshita M, Kopidakis N, Bothe K, Siefert G, Hao X (2023) Solar cell efficiency tables (Version 63). *Prog Photovolt Res Appl* n/a. <https://doi.org/10.1002/pip.3750>
- [19] Almora O, Baran D, Bazan GC, Cabrera CI, Erten-Ela S, Forberich K, Guo F, Hauch J, Ho-Baillie AWY, Jacobsson TJ, Janssen RAJ, Kirchartz T, Kopidakis N, Loi MA, Lunt RR, Mathew X, McGehee MD, Min J, Mitzi DB, Nazeeruddin MK, Nelson J, Nogueira AF, Paetzold UW, Rand BP, Rau U, Snaith HJ, Unger E, Vaillant-Roca L, Yang C, Yip H-L, Brabec CJ (2023) Device performance of emerging photovoltaic materials (version 3). *Adv Energy Mater* 13:2203313. <https://doi.org/10.1002/aenm.202203313>
- [20] Lee J-H, Bristowe NC, Lee JH, Lee S-H, Bristowe PD, Cheetham AK, Jang HM (2016) Resolving the physical origin of octahedral tilting in halide perovskites. *Chem Mater* 28:4259–4266. <https://doi.org/10.1021/acs.chemmater.6b00968>
- [21] Svane KL, Forse AC, Grey CP, Kieslich G, Cheetham AK, Walsh A, Butler KT (2017) How strong is the hydrogen bond in hybrid perovskites? *J Phys Chem Lett* 8:6154–6159. <https://doi.org/10.1021/acs.jpcclett.7b03106>
- [22] Quarti C, Mosconi E, De Angelis F (2014) Interplay of orientational order and electronic structure in methylammonium lead iodide: implications for solar cell operation. *Chem Mater* 26:6557–6569. <https://doi.org/10.1021/cm5032046>
- [23] Filip MR, Eperon GE, Snaith HJ, Giustino F (2014) Steric engineering of metal-halide perovskites with tunable optical band gaps. *Nat Commun* 5:5757. <https://doi.org/10.1038/ncomms6757>
- [24] Egger DA, Kronik L (2014) Role of dispersive interactions in determining structural properties of organic-inorganic halide perovskites: insights from first-principles calculations. *J Phys Chem Lett* 5:2728–2733. <https://doi.org/10.1021/jz5012934>
- [25] El-Mellouhi F, Marzouk A, Bentría ET, Rashkeev SN, Kais S, Alharbi FH (2016) Hydrogen bonding and stability of hybrid organic-inorganic perovskites. *Chemoschem* 9:2648–2655. <https://doi.org/10.1002/cssc.201600864>
- [26] Lee JH, Lee J-H, Kong E-H, Jang HM (2016) The nature of hydrogen-bonding interaction in the prototypic hybrid halide perovskite, tetragonal CH<sub>3</sub>NH<sub>3</sub>PbI<sub>3</sub>. *Sci Rep* 6:21687. <https://doi.org/10.1038/srep21687>
- [27] Jiang J, Liu F, Tranca I, Shen Q, Tao S (2020) Atomistic and electronic origin of phase instability of metal halide perovskites. *ACS Appl Energy Mater* 3:11548–11558. <https://doi.org/10.1021/acsaem.0c00791>



- [28] Guo L, Tang G, Hong J (2019) Mechanical properties of formamidinium halide perovskites FABX<sub>3</sub> (FA=CH(NH<sub>2</sub>)<sub>2</sub>; B=Pb, Sn; X=Br, I) by first-principles calculations\*. *Chin Phys Lett* 36:56201. <https://doi.org/10.1088/0256-307X/36/5/056201>
- [29] Ornelas-Cruz I, González I, Pilo J, Trejo A, Oviedo-Roa R, Cruz-Irisson M (2022) Impact of alkaline-earth doping on electronic properties of the photovoltaic perovskite CsSnI<sub>3</sub>: insights from a DFT perspective. *Dalt Trans* 51:6607–6621. <https://doi.org/10.1039/D1DT04041C>
- [30] Snaith HJ (2018) Present status and future prospects of perovskite photovoltaics. *Nat Mater* 17:372–376. <https://doi.org/10.1038/s41563-018-0071-z>
- [31] Delley B (2000) From molecules to solids with the DMol3 approach. *J Chem Phys* 113:7756–7764. <https://doi.org/10.1063/1.1316015>
- [32] Perdew JP, Burke K, Ernzerhof M (1996) Generalized gradient approximation made simple. *Phys Rev Lett* 77:3865–3868. <https://doi.org/10.1103/PhysRevLett.77.3865>
- [33] Delley B (1990) An all-electron numerical method for solving the local density functional for polyatomic molecules. *J Chem Phys* 92:508–517. <https://doi.org/10.1063/1.458452>
- [34] Delley B (2002) Hardness conserving semilocal pseudopotentials. *Phys Rev B* 66:155125. <https://doi.org/10.1103/PhysRevB.66.155125>
- [35] Monkhorst HJ, Pack JD (1976) Special points for Brillouin-zone integrations. *Phys Rev B* 13:5188–5192. <https://doi.org/10.1103/PhysRevB.13.5188>
- [36] Tao J, Perdew JP, Staroverov VN, Scuseria GE (2003) climbing the density functional ladder: nonempirical meta-generalized gradient approximation designed for molecules and solids. *Phys Rev Lett* 91:146401. <https://doi.org/10.1103/PhysRevLett.91.146401>
- [37] Perdew JP, Ruzsinszky A, Csonka GI, Constantin LA, Sun J (2009) Workhorse Semilocal density functional for condensed matter physics and quantum chemistry. *Phys Rev Lett* 103:26403. <https://doi.org/10.1103/PhysRevLett.103.026403>
- [38] Peverati R, Truhlar DG (2012) Exchange–correlation functional with good accuracy for both structural and energetic properties while depending only on the density and its gradient. *J Chem Theory Comput* 8:2310–2319. <https://doi.org/10.1021/ct3002656>
- [39] Tkatchenko A, Scheffler M (2009) Accurate molecular van der waals interactions from ground-state electron density and free-atom reference data. *Phys Rev Lett* 102:73005. <https://doi.org/10.1103/PhysRevLett.102.073005>
- [40] Miller GJ, Zhang Y, Wagner FR, 2017 Chemical bonding in solids. In: *Handbook of solid state Chemistry*, <https://doi.org/10.1002/9783527691036.hsscvol5013>
- [41] Görne AL, Dronskowski R (2019) Covalent bonding versus total energy: on the attainability of certain predicted low-energy carbon allotropes. *Carbon N Y* 148:151–158. <https://doi.org/10.1016/j.carbon.2019.03.070>
- [42] George J, Petretto G, Naik A, Esters M, Jackson AJ, Nelson R, Dronskowski R, Rignanese G-M, Hautier G (2022) Automated bonding analysis with crystal orbital hamilton populations. *ChemPlusChem* 87:e202200123. <https://doi.org/10.1002/cplu.202200123>
- [43] Weller MT, Weber OJ, Henry PF, Di Pumpo AM, Hansen TC (2015) Complete structure and cation orientation in the perovskite photovoltaic methylammonium lead iodide between 100 and 352 K. *Chem Commun* 51:4180–4183. <https://doi.org/10.1039/C4CC09944C>
- [44] Weller MT, Weber OJ, Frost JM, Walsh A (2015) Cubic perovskite structure of black formamidinium lead iodide,  $\alpha$ -[HC(NH<sub>2</sub>)<sub>2</sub>]PbI<sub>3</sub>, at 298 K. *J Phys Chem Lett* 6:3209–3212. <https://doi.org/10.1021/acs.jpcclett.5b01432>
- [45] Trots DM, Myagkota SV (2008) High-temperature structural evolution of caesium and rubidium triiodoplumbates. *J Phys Chem Solids* 69:2520–2526. <https://doi.org/10.1016/j.jpcs.2008.05.007>
- [46] Eperon GE, Paternò GM, Sutton RJ, Zampetti A, Haghighirad AA, Cacialli F, Snaith HJ (2015) Inorganic caesium lead iodide perovskite solar cells. *J Mater Chem A* 3:19688–19695. <https://doi.org/10.1039/C5TA06398A>
- [47] Chen T, Foley BJ, Park C, Brown CM, Harriger LW, Lee J, Ruff J, Yoon M, Choi JJ, Lee S-H (2022) Entropy-driven structural transition and kinetic trapping in formamidinium lead iodide perovskite. *Sci Adv* 2:e1601650. <https://doi.org/10.1126/sciadv.1601650>
- [48] Hui W, Chao L, Lu H, Xia F, Wei Q, Su Z, Niu T, Tao L, Du B, Li D, Wang Y, Dong H, Zuo S, Li B, Shi W, Ran X, Li P, Zhang H, Wu Z, Ran C, Song L, Xing G, Gao X, Zhang J, Xia Y, Chen Y, Huang W (2021) Stabilizing black-phase formamidinium perovskite formation at room temperature and high humidity. *Science* 371:1359–1364. <https://doi.org/10.1126/science.abf7652>
- [49] Tao SX, Cao X, Bobbert PA (2017) Accurate and efficient band gap predictions of metal halide perovskites using the DFT-1/2 method: GW accuracy with DFT expense. *Sci Rep* 7:14386. <https://doi.org/10.1038/s41598-017-14435-4>
- [50] dos Santos RM, Da Ornelas-CruzDiasLimaSilva IAC-MPJLF (2023) Theoretical investigation of the role of mixed a+ cations in the structure, stability, and electronic properties of perovskite alloys. *ACS Appl Energy Mater* 6:5259–5273. <https://doi.org/10.1021/acsaem.3c00186>
- [51] Srikanth M, Ozório MS, Da Silva JLF (2020) Optical and dielectric properties of lead perovskite and iodoplumbate

- complexes: an ab initio study. *Phys Chem Chem Phys* 22:18423–18434. <https://doi.org/10.1039/D0CP03512B>
- [52] Tao S, Schmidt I, Brocks G, Jiang J, Tranca I, Meerholz K, Olthof S (2019) Absolute energy level positions in tin- and lead-based halide perovskites. *Nat Commun* 10:2560. <https://doi.org/10.1038/s41467-019-10468-7>
- [53] Ornelas-Cruz I, Trejo A, Oviedo-Roa R, Salazar F, Carvajal E, Miranda A, Cruz-Irisson M (2020) DFT-based study of the bulk tin mixed-halide CsSnI<sub>3</sub>-xBr<sub>x</sub> perovskite. *Comput Mater Sci* 178:109619. <https://doi.org/10.1016/j.commat.2020.109619>
- [54] Varadwaj PR, Varadwaj A, Marques HM, Yamashita K (2019) Significance of hydrogen bonding and other noncovalent interactions in determining octahedral tilting in the CH<sub>3</sub>NH<sub>3</sub>PbI<sub>3</sub> hybrid organic-inorganic halide perovskite solar cell semiconductor. *Sci Rep* 9:50. <https://doi.org/10.1038/s41598-018-36218-1>
- [55] Tu Q, Kim D, Shyikh M, Kanatzidis MG (2021) Mechanics-coupled stability of metal-halide perovskites. *Matter* 4:2765–2809. <https://doi.org/10.1016/j.matt.2021.06.028>
- [56] Marronnier A, Lee H, Geffroy B, Even J, Bonnassieux Y, Roma G (2017) Structural instabilities related to highly anharmonic phonons in halide perovskites. *J Phys Chem Lett* 8:2659–2665. <https://doi.org/10.1021/acs.jpcclett.7b00807>
- [57] Yin W-J, Yan Y, Wei S-H (2014) Anomalous alloy properties in mixed halide perovskites. *J Phys Chem Lett* 5:3625–3631. <https://doi.org/10.1021/jz501896w>
- [58] Arunan E, Desiraju GR, Klein RA, Sadlej J, Scheiner S, Alkorta I, Clary DC, Crabtree RH, Dannenberg JJ, Hobza P, Kjaergaard HG, Legon AC, Mennucci B, Nesbitt DJ (2011) Definition of the hydrogen bond (IUPAC recommendations 2011). *Pure Appl Chem* 83:1637–1641. <https://doi.org/10.1351/PAC-REC-10-01-02>
- [59] Manser JS, Christians JA, Kamat PV (2016) Intriguing optoelectronic properties of metal halide perovskites. *Chem Rev* 116:12956–13008. <https://doi.org/10.1021/acs.chemrev.6b00136>
- [60] Medvedev MG, Bushmarinov IS, Sun J, Perdew JP, Lyssenko KA (2017) Density functional theory is straying from the path toward the exact functional. *Science* 355:49–52. <https://doi.org/10.1126/science.aah5975>
- [61] Mardirossian N, Head-Gordon M (2017) Thirty years of density functional theory in computational chemistry: an overview and extensive assessment of 200 density functionals. *Mol Phys* 115:2315–2372. <https://doi.org/10.1080/00268976.2017.1333644>
- [62] Wang H, Tal A, Bischoff T, Gono P, Pasquarello A (2022) Accurate and efficient band-gap predictions for metal halide perovskites at finite temperature. *Npj Comput Mater* 8:237. <https://doi.org/10.1038/s41524-022-00869-6>
- [63] Rojas-Chávez H, Miralrio A, Hernández-Rodríguez Y, Cruz-Martínez H, Pérez-Pérez R, Cigarroa-Mayorga O (2021) Needle- and cross-linked ZNO microstructures and their photocatalytic activity using experimental and DFT approach. *Mater Lett* 291:129474. <https://doi.org/10.1016/j.matlet.2021.129474>

**Publisher's Note** Springer Nature remains neutral with regard to jurisdictional claims in published maps and institutional affiliations.